Available online at www.sciencedirect.com
ScienceDirect
International Journal of Multiphase Flow 34 (2008) 437–446
International Journal of Multiphase Flow
www.elsevier.com/locate/ijmulflow

One-, two-, and three-dimensional solutions for counter-current steady-state two-phase subsurface flow

F.T. Tracy *

US Army Engineer Research and Development Center, 3909 Halls Ferry Road, Vicksburg, MS 39180, USA

Received 1 August 2006; received in revised form 2 February 2007

Abstract

This paper derives analytical solutions for steady-state one-dimensional (1-D), two-dimensional (2-D), and three-dimensional (3-D) two-phase immiscible subsurface flow for a counter-current problem. Since the governing equations are highly nonlinear, 2-D and 3-D derivations are generally difficult to obtain. The primary purpose for the solutions is to test finite difference/volume/element computer programs for accuracy and scalability using architectures ranging from PCs to parallel high performance computers. This derivation is accomplished by first solving for the saturation of water in terms of a function that is a solution to Laplace's equation to achieve a set of partial differential equations that allows some degree of latitude in the choice of boundary conditions. Separation of variables and Fourier series are used to obtain the final solution. The test problem consists of a rectangular block of soil where specified pressure is applied at the top and bottom of the sample, and no-flow boundary conditions are imposed on the sides. The pressure at the top of the sample is a step function that allows the testing of adaptive meshing or concentration of grid points in action zones.
© 2008 Published by Elsevier Ltd.

Keywords: Two-phase subsurface flow; Oil–water modeling; Analytical solutions; Testing numerical models

1. Introduction

The computer programs used to model two-phase groundwater flow need tools to test their accuracy and efficiency. One such tool is analytical solutions When the governing partial differential equations (PDEs) are highly nonlinear, these analytical solutions are generally difficult to obtain. This is certainly true of two-phase flow where not only the equations for oil and water are highly nonlinear, but they are also coupled. Some one-dimensional (1-D) solutions exist for vertical flow, but two-dimensional (2-D) and three-dimensional (3-D) solutions are rare. This paper derives analytical solutions for steady-state 1-D, 2-D and 3-D two-phase oil–water subsurface flow having counter-current velocities.

2. Previous work

Sander et al. (1988) derived an analytical nonlinear solution to the problem of 1-D two-phase oil and water infiltration under a constant flux boundary condition. By using a very simple change in the independent variables of space and time, this solution was shown to also apply to the problem of constant infiltration of water. Yang (1992) built upon this work and found an analytical solution to two-phase flow of up to three dimensions where the solution is exact when the total mobility of the two phases is a constant. The solution was derived from basic continuity equations using the method of characteristics. The solution includes the effects from production rate, relative permeability curve, viscosity, well configuration, formation anisotropy, and boundaries. One important application of this solution is to the evaluation of water coning into vertical or horizontal wells. Tsai (1990) discusses an analytical solution of dense two-phase flow in a vertical pipeline. Hewett and Yamada (1997) developed a semianalytical

* Tel.: +1 601 634 4112; fax: +1 601 634 2324.
E-mail address: Fred.T.Tracy@.usace.army.mil

0301-9322/$ - see front matter © 2008 Published by Elsevier Ltd.
doi:10.1016/j.ijmultiphaseflow.2007.02.011

method for calculating oil recovery in two and three dimensions and for calculating effective relative permeabilities for coarse grids. The calculations are based on the assumption that the effects of a changing mobility field can be accounted for by using fixed streamtube geometries with flow rates updated to account for the changing mobility distribution. Walter (1990) gives analytical descriptions of idealized two-phase flow of immiscible fluids in capillary pore spaces shaped like cylinders and cracks. Panfilov and Floriat (2004) derived a macroscale model of first-order for two-phase immiscible flow through a heterogeneous porous medium in a gravity field but with neglected capillary pressure. Iqbal and Civan (1986) discuss the finite analytic method for reservoir flow models. These techniques combine analytical methods with computational schemes to potentially be more accurate than conventional finite difference and finite element methods. However, they are naturally problem-dependent. Jinno (1978) derived equations for the finite element method using the 1-D equations for the two-phase interface of the free surface and extended his method to two dimensions. Hou (2005) did a multiscale analysis that provides a useful guideline for designing effective numerical methods for incompressible flow by (1) constructing local multiscale bases for diffusion-dominated problems good for two-phase flow in heterogeneous porous media and (2) deriving semianalytic multiscale solutions local in space and time whose solutions approximate large-scale convection-dominated transport. The phenomenon of instabilities (fingering) was investigated by Verma and Mishra (1973), and an analytical expression for the average cross-sectional area occupied by fingers was derived and applied to fingering stabilization. Cai and Zhang (2001) derived two sets of algebraically explicit analytical solutions for 1-D unsteady gas–liquid two-phase flow. Okusu and Udell (1989) derived a semianalytical model of steady, 1-D immiscible displacement that includes the effects of capillarity and gravity. The solution divides the two-phase zone into two regions: a stabilized zone where the saturations propagate at a constant velocity and a multivelocity zone. In the stabilized zone, the equations of multiphase flow are transformed onto a moving coordinate system, and a first-order, ordinary differential equation describing the change in saturation is obtained. The fractional flow (the ratio of injected phase velocity to the total velocity) including capillarity is shown to be linear with respect to saturation in this region. Constitutive equations for the wetting and nonwetting phase pressures are then derived. Finally, Tracy (1997) compares two-phase flow computations using analytical solutions and finite element models, which is the genesis of the work presented in this paper.

3. Governing equations

Steady-state flow in a homogeneous porous medium of two immiscible fluids with constant densities with the wetting phase represented by water and the nonwetting phase represented by oil is given by

$$\nabla \cdot (K_w \nabla h_w) + \frac{\partial K_w}{\partial z} = 0 \tag{1}$$

$$\nabla \cdot (K_o \nabla h_o) + \frac{\partial K_o}{\partial z} = 0 \tag{2}$$

where h_w is the pressure head of the water, h_o is the pressure head of the oil, K_w is the hydraulic conductivity of water, K_o is the hydraulic conductivity of oil, z is the z coordinate, and

$$h_w = \frac{p_w}{\rho_w g} \tag{3}$$

$$h_o = \frac{p_o}{\rho_o g} \tag{4}$$

where p_w is the pressure of the water, p_o is the pressure of the oil, ρ_w is the density of the water, ρ_o is the density of the oil, and g is the acceleration because of gravity. One should note carefully that h_w and h_o are defined using different densities. Hydraulic conductivity is modeled by

$$K_w = k_{wr} K_{ws} \tag{5}$$

$$K_o = k_{or} K_{os} \tag{6}$$

where K_{ws} is the saturated hydraulic conductivity of water, k_{wr} is the relative hydraulic conductivity of water, K_{os} is the saturated hydraulic conductivity of oil, and k_{or} is the relative hydraulic conductivity of oil. k_{wr} and k_{or} are the terms that cause the nonlinearity in the governing equations. Eqs. (1) and (2) can now be written

$$\frac{\partial k_{wr}}{\partial z} + \nabla \cdot (k_{wr} \nabla h_w) = 0 \tag{7}$$

$$\frac{\partial k_{or}}{\partial z} + \nabla \cdot (k_{or} \nabla h_w) - \nabla \cdot (k_{or} \nabla h_c) = 0, \quad h_c = h_w - h_o \tag{8}$$

where h_c is the capillary pressure.

4. Relative hydraulic conductivity and moisture content

Relative hydraulic conductivity for water is modeled by a version of Gardner's exponential model (Gardner, 1958; Seǵol, 1994) as follows:

$$k_{wr} = e^{\alpha h_c} \tag{9}$$

where α is a parameter. This is the basis of the quasi-linear assumption that is illustrated well by Warrick (2003) and is useful for deriving analytical solutions for unsaturated flow.

Irmay (1954) determined experimentally that some unsaturated soils can be modeled using

$$k_{wr} = S^m, \quad S = \frac{\theta_w - \theta_r}{\theta_s - \theta_r} \tag{10}$$

where S is the saturation of water, θ_w is the water content, θ_s is the saturated liquid content, θ_r is the residual liquid content, and m is a parameter. For simplicity in this derivation, $m = 1$ is chosen. Then

$$\theta_w = \theta_r + (\theta_s - \theta_r) e^{\alpha h_c} \tag{11}$$

Fig. 1 compares Eq. (11) to the more standard equation by van Genuchten (1980),

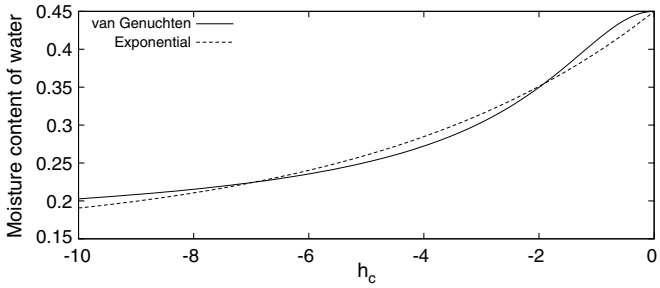

Fig. 1. Water content for van Genuchten and exponential models.

$$\theta_w = \theta_r + \frac{\theta_s - \theta_r}{[1 + (-\xi h_c)^n]^{1-\frac{1}{n}}} \tag{12}$$

for $\xi = 0.56\ \mathrm{m}^{-1}$, $n = 2.0$, $\theta_r = 0.15$, $\theta_s = 0.45$, and $\alpha = 0.20\ \mathrm{m}^{-1}$. The curves are close enough for testing numerical models. The use of Eq. (10) can be justified by realizing first that unsaturated flow is two-phase flow with water and air. Since the pressure due to air is usually taken as zero, the pressure head of water is the capillary pressure. Thus, curves such as the van Genuchten equation are used for unsaturated flow and two-phase flow, too. The use of the simple equations,

$$k_{wr} = S \tag{13}$$

$$S = e^{\alpha h_c} \quad \text{or} \quad h_c = \frac{1}{\alpha} \ln S \tag{14}$$

is done because this is the relationship that allows the analytical solution to be achieved. This does greatly limit the soils that apply, but since the goal of this work is to test numerical models, this is an acceptable approximation.

In like manner,

$$k_{or} = 1 - S \tag{15}$$

5. General solution

First, substituting Eqs. (13)–(15) into Eqs. (7) and (8) produces

$$\frac{\partial S}{\partial z} + \nabla \cdot (S \nabla h_w) = 0 \tag{16}$$

$$-\frac{\partial S}{\partial z} + \nabla \cdot [(1-S)\nabla h_w] - \frac{1}{\alpha} \nabla \cdot \left[\frac{(1-S)}{S} \nabla S \right] = 0 \tag{17}$$

The sum of Eqs. (16) and (17) yields

$$\nabla \cdot \left[\nabla h_w - \frac{1}{\alpha} \frac{(1-S)}{S} \nabla S \right] = 0 \tag{18}$$

or

$$\nabla^2 \left(h_w - \frac{1}{\alpha} \ln S + \frac{1}{\alpha} S \right) = 0 \tag{19}$$

This gives

$$h_w - \frac{1}{\alpha} \ln S + \frac{1}{\alpha} S = \phi, \qquad \nabla^2 \phi = 0 \tag{20}$$

Putting Eq. (14) into Eq. (20) generates

$$h_o + \frac{1}{\alpha} S = \phi \tag{21}$$

5.1. Determination of ϕ

The solutions provided in this paper are limited to those where

$$\phi = -z + c_0 \tag{22}$$

where c_0 is a constant determined from the boundary conditions. Substituting Eq. (22) into Eqs. (20) and (21) gives

$$h_w = \frac{1}{\alpha} \ln S - \frac{1}{\alpha} S - z + c_0 \tag{23}$$

$$h_o = -\frac{1}{\alpha} S - z + c_0 \tag{24}$$

The justification for using Eq. (22) is that this simplification allows an easy derivation for S. The impact of this choice is that the total heads and Darcy velocities for both oil and water depend only on S. These criteria are met in the test problem given below.

Another way to understand the impact of Eq. (22) is to examine the dimensionless "total velocity,"

$$\mathbf{V} = \frac{\mathbf{V}_w}{K_{ws}} + \frac{\mathbf{V}_o}{K_{os}} \tag{25}$$

where $\mathbf{V}_w$ is the Darcy velocity for water, and $\mathbf{V}_o$ is the Darcy velocity for oil. From the definition of Eq. (25).

$$\mathbf{V} = -k_{wr} \nabla (h_w + z) - k_{or} \nabla (h_o + z) \tag{26}$$

From Eqs. (23) and (24), (26) becomes

$$\mathbf{V} = S \nabla \left(-\frac{1}{\alpha} \ln S + \frac{1}{\alpha} S \right) + (1-S) \nabla \left(\frac{1}{\alpha} S \right) \tag{27}$$

The conclusion of the meaning of Eq. (22) from Eq. (27) is that

$$\mathbf{V} = 0 \tag{28}$$

This means a counter-current flow of water and oil while the oil and water velocities are inversely proportional to the corresponding hydraulic conductivities, K_{ws} and K_{os}, respectively. To elaborate, combining Eqs. (25) and (28) gives

$$K_{ws}\mathbf{V}_o + K_{os}\mathbf{V}_w = \zeta_1 + \zeta_2 = 0 \tag{29}$$

where ζ_1 and ζ_2 are proportionality constants. When $\zeta_1 = -\zeta_2$, counter-current flow occurs. In particular, if the oil and water properties are identical, then Eq. (28) means simply a counter-current flow at equivalent absolute phase velocities at each point.

5.2. Derivation of S

By substituting Eq. (23) into Eq. (16),

$$\frac{\partial S}{\partial z} + \frac{1}{\alpha}\nabla\cdot[(1-S)\nabla S] - \nabla\cdot(S\nabla z) = 0 \tag{30}$$

or

$$\nabla\cdot[(1-S)\nabla S] = 0 \tag{31}$$

or

$$\nabla^2[(1-S)^2] = 0 \tag{32}$$

or

$$(1-S)^2 = \psi, \quad \nabla^2\psi = 0 \tag{33}$$

The general solution for S is therefore

$$S = 1 - \sqrt{\psi}, \quad 0 \leqslant \psi \leqslant 1 \tag{34}$$

The final solution is now reduced to solving Laplace's equation for ψ based on the boundary conditions.

6. Test problem

Since the goal is to test numerical programs, geometrically simple problems are selected. A rectangular block of soil having dimensions $a \times b \times L$ with $0 \leqslant x \leqslant a$, $0 \leqslant y \leqslant b$, $0 \leqslant z \leqslant L$ will now be considered as shown in Fig. 2. Pressure head is specified at the bottom and top of the soil sample, and the sides are impervious. Water is applied in the middle fourth at the top plane ($z = L$) (see Fig. 2). The boundary conditions are designed so that water flows downward, and oil flows upward. With only the need to satisfy Eq. (22) and for ψ to satisfy Laplace's equation, a wide range of problems can be solved using separation of variables and Fourier series. The resulting boundary conditions for one such problem where the pressure head for oil at the top-left and top-right of the soil sample (not in the middle) is chosen to be zero are as follows:

$$\begin{aligned}
&k_{wr}(x,y,0) = \epsilon_1, \quad 0 < \epsilon_1 < \frac{1}{2}\\
&h_o(x,y,0) = L\\
&h_w(x,y,0) = \frac{1}{\alpha}\ln[k_{wr}(x,y,0)] + h_o(x,y,0)
\end{aligned} \tag{35}$$

$$\begin{aligned}
k_{wr}(x,y,L) = \epsilon_1 + (1-\epsilon_1-\epsilon_2)&\left[U\left(x-\frac{a}{4}\right) - U\left(x-\frac{3a}{4}\right)\right]\\
&\times\left[U\left(y-\frac{b}{4}\right) - U\left(y-\frac{3b}{4}\right)\right], \quad 0 \leqslant \epsilon_2 < \frac{1}{2}\\
h_o(x,y,L) = \frac{\epsilon_1 - k_{wr}(x,y,L)}{\alpha}&\\
h_w(x,y,L) = \frac{1}{\alpha}\ln[k_{wr}(x,y,L)] + h_o(x,y,L)&
\end{aligned} \tag{36}$$

where U is the unity step function.

$$\begin{aligned}
&\frac{\partial h_w}{\partial x}(0,y,z) = \frac{\partial h_o}{\partial x}(0,y,z) = 0\\
&\frac{\partial h_w}{\partial x}(a,y,z) = \frac{\partial h_o}{\partial x}(a,y,z) = 0\\
&\frac{\partial h_w}{\partial y}(x,0,z) = \frac{\partial h_o}{\partial y}(x,0,z) = 0\\
&\frac{\partial h_w}{\partial y}(x,b,z) = \frac{\partial h_o}{\partial y}(x,b,z) = 0
\end{aligned} \tag{37}$$

There is no particular need to start with defining relative hydraulic conductivities; it is just convenient. Also, the step function aspect of the top boundary condition allows for the testing of adaptive meshing or concentration of grid points near action zones.

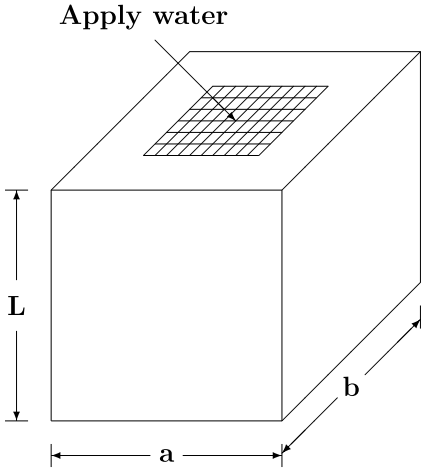

Fig. 2. Test problem.

7. 1-D flow

Consider 1-D vertical flow along the line $x = \frac{a}{2}, y = \frac{b}{2}$. Using Eq. (24) at $z = 0$, c_o becomes

$$c_o = L + \frac{\epsilon_1}{\alpha} \tag{38}$$

From Eq. (34)

$$\psi = (1 - S)^2 \tag{39}$$

which provides

$$\begin{aligned} \psi(0) &= (1 - \epsilon_1)^2 \\ \psi(L) &= \epsilon_2^2 \end{aligned} \tag{40}$$

The solution of Laplace's equation for ψ that matches the above boundary conditions is

$$\psi = (1 - \epsilon_1)^2 \left(\frac{L - z}{L}\right) + \epsilon_2^2 \left(\frac{z}{L}\right) \tag{41}$$

7.1. Pressure head

The solution for pressure head can now be summarized as follows:

$$\begin{aligned} \psi &= (1 - \epsilon_1)^2 \left(\frac{L - z}{L}\right) + \epsilon_2^2 \left(\frac{z}{L}\right) \\ S &= 1 - \sqrt{\psi} \\ h_o &= \frac{1}{\alpha}(\epsilon_1 - S) + L - z \\ h_w &= \frac{1}{\alpha} \ln S + h_o \end{aligned} \tag{42}$$

7.2. Water and oil content

Water and oil contents are computed by

$$\begin{aligned} \theta_w &= \theta_r + (\theta_s - \theta_r) S \\ \theta_o &= \theta_s - \theta_w \end{aligned} \tag{43}$$

7.3. Darcy velocity

Darcy velocity is computed by

$$\begin{aligned} v_o &= -K_o \left(\frac{dh_o}{dz} + 1\right) \\ &= \frac{K_o}{\alpha}\left(\frac{dS}{dz}\right) \\ &= \frac{K_{os}}{\alpha}(1 - S)\left(\frac{dS}{dz}\right) \\ &= \frac{K_{os}}{\alpha}\left(\sqrt{\psi}\right)\left(-\frac{1}{2\sqrt{\psi}}\right)\left(\frac{d\psi}{dz}\right) \\ &= \frac{K_{os}}{2\alpha L}[(1 - \epsilon_1)^2 - \epsilon_2^2] \end{aligned} \tag{44}$$

$$\begin{aligned} v_w &= -K_w \left(\frac{dh_w}{dz} + 1\right) \\ &= -\frac{K_{ws}}{\alpha} S \left(\frac{1}{S} - 1\right)\frac{dS}{dz} \\ &= -\frac{K_{ws}}{\alpha}\left(\sqrt{\psi}\right)\left(-\frac{1}{2\sqrt{\psi}}\right)\left(\frac{d\psi}{dz}\right) \\ &= -\frac{K_{ws}}{2\alpha L}[(1 - \epsilon_1)^2 - \epsilon_2^2] \end{aligned} \tag{45}$$

Therefore, in this simple 1-D case, the Darcy velocities are constant. However, $K_{ws} = K_{os}$ is required for total flux or mobility to be zero.

8. 2-D flow

2-D flow in the plane $y = \frac{b}{2}$ will now be derived. As seen in the 1-D case, computing ψ is the primary challenge. First, at $x = 0$, Eq. (14) gives

$$\frac{\partial S}{\partial x}(0, z) = \alpha e^{\alpha h_c}\left[\frac{\partial h_w}{\partial x}(0, z) - \frac{\partial h_o}{\partial x}(0, z)\right] = 0 \tag{46}$$

From Eq. (34),

$$\frac{\partial S}{\partial x}(0, z) = -\frac{1}{2\sqrt{\psi}}\frac{\partial \psi}{\partial x}(0, z) \tag{47}$$

Combining the two equations above gives

$$\frac{\partial \psi}{\partial x}(0, z) = 0 \tag{48}$$

The boundary conditions for ψ are therefore

$$\begin{aligned} \psi(x, 0) &= (1 - \epsilon_1)^2 \\ \frac{\partial \psi}{\partial x}(0, z) &= \frac{\partial \psi}{\partial x}(a, z) = 0 \\ \psi(x, L) &= (1 - \epsilon_1)^2 - [(1 - \epsilon_1)^2 - \epsilon_2^2] \\ &\quad \times \left[U\left(x - \frac{a}{4}\right) - U\left(x - \frac{3a}{4}\right)\right] \end{aligned} \tag{49}$$

The solution of Laplace's equation for ψ can be determined by separation of variables for this type boundary condition as shown by Tracy (2006) and is as follows:

$$\psi = (1 - \epsilon_1)^2 + A_0 z + \sum_{i=1}^{\infty} A_i \cos(\lambda_i x) \sinh(\lambda_i z) \tag{50}$$

where

$$\lambda_i = \frac{i\pi}{a} \tag{51}$$

A_i can be determined using a half-range Fourier cosine series and evaluating Eq. (50) at $z = L$. So

$$A_0 = -\frac{(1 - \epsilon_1)^2 - \epsilon_2^2}{2L} \tag{52}$$

and

Table 1
2-D solution

Variable	Equation
$k_{wr}(x,0)$	ϵ_1
$h_o(x,0)$	L
$h_w(x,0)$	$\frac{1}{\alpha}\ln[k_{wr}(x,0)]+h_o(x,0)$
$k_{wr}(x,L)$	$\epsilon_1+(1-\epsilon_1-\epsilon_2)\left[U\left(x-\frac{a}{4}\right)-U\left(x-\frac{3a}{4}\right)\right]$
$h_o(x,L)$	$\frac{\epsilon_1-k_{wr}(x,L)}{\alpha}$
$h_w(x,L)$	$\frac{1}{\alpha}\ln[k_{wr}(x,L)]+h_o(x,L)$
λ_{4i-2}	$\frac{(4i-2)\pi}{a}$
ψ	$(1-\epsilon_1)^2+[(1-\epsilon_1)^2-\epsilon_2^2]\left[-\frac{z}{2L}.+\frac{4}{\pi}\sum_{i=1}^{\infty}\frac{(-1)^{i+1}}{4i-2}\cos(\lambda_{4i-2}x)\frac{\sinh(\lambda_{4i-2}z)}{\sinh(\lambda_{4i-2}L)}\right]$
S	$1-\sqrt{\psi}$
h_o	$\frac{1}{\alpha}(\epsilon_1-S)+L-z$
h_w	$\frac{1}{\alpha}\ln S+h_o$
θ_w	$\theta_r+(\theta_s-\theta_r)S$
θ_o	$\theta_s-\theta_w$
v_{ox}	$\frac{2K_{os}[(1-\epsilon_1)^2-\epsilon_2^2]}{\pi a}\sum_{i=1}^{\infty}(-1)^{i+1}\sin(\lambda_{4i-2}x)\frac{\sinh(\lambda_{4i-2}z)}{\sinh(\lambda_{4i-2}L)}$
v_{wx}	$\frac{2K_{ws}[(1-\epsilon_1)^2-\epsilon_2^2]}{\pi a}\sum_{i=1}^{\infty}(-1)^{i}\sin(\lambda_{4i-2}x)\frac{\sinh(\lambda_{4i-2}z)}{\sinh(\lambda_{4i-2}L)}$
v_{oz}	$\frac{K_{os}[(1-\epsilon_1)^2-\epsilon_2^2]}{\alpha}\left[\frac{1}{4L}.+\frac{2}{a}\sum_{i=1}^{\infty}(-1)^{i}\cos(\lambda_{4i-2}x)\frac{\cosh(\lambda_{4i-2}z)}{\sinh(\lambda_{4i-2}L)}\right]$
v_{ow}	$\frac{K_{os}[(1-\epsilon_1)^2-\epsilon_2^2]}{\alpha}\left[-\frac{1}{4L}.+\frac{2}{a}\sum_{i=1}^{\infty}(-1)^{i+1}\cos(\lambda_{4i-2}x)\frac{\cosh(\lambda_{4i-2}z)}{\sinh(\lambda_{4i-2}L)}\right]$

$$A_i=-\frac{2[(1-\epsilon_1)^2-\epsilon_2^2]}{a\sinh(\lambda_iL)}\int_{\frac{a}{4}}^{\frac{3a}{4}}\cos(\lambda_ix)\mathrm{d}x$$
$$=-\frac{2[(1-\epsilon_1)^2-\epsilon_2^2]}{i\pi\sinh(\lambda_iL)}\left[\sin\left(\frac{3i\pi}{4}\right)-\sin\left(\frac{i\pi}{4}\right)\right] \quad (53)$$

Only the second and sixth term out of every eight terms of A_i are nonzero, so the final result for ψ is now written

$$\psi=(1-\epsilon_1)^2+[(1-\epsilon_1)^2-\epsilon_2^2]\times\left[-\frac{z}{2L}+\frac{4}{\pi}\sum_{i=1}^{\infty}\frac{(-1)^{i+1}}{4i-2}\cos(\lambda_{4i-2}x)\frac{\sinh(\lambda_{4i-2}z)}{\sinh(\lambda_{4i-2}L)}\right] \quad (54)$$

As seen in the 1-D case, once ψ has been computed, the rest of the solution falls quickly in place. Table 1 gives a summary of the results.

9. Convergence of solution

Eq. (54) converges very rapidly and absolutely for $0\leqslant z<L$. Consider the term of the series,

$$A_i=\frac{(-1)^{i+1}}{4i-2}\cos(\lambda_{4i-2}x)\frac{\sinh(\lambda_{4i-2}z)}{\sinh(\lambda_{4i-2}L)} \quad (55)$$

Then,

$$|A_i|\leqslant B_i=\left(\frac{1}{4i-2}\right)\frac{\sinh(\lambda_{4i-2}z)}{\sinh(\lambda_{4i-2}L)} \quad (56)$$

Now,

$$\lim_{i\to\infty}B_i=\lim_{i\to\infty}\left[\left(\frac{1}{4i-2}\right)\frac{\mathrm{e}^{\lambda_{4i-2}(z-L)}-\mathrm{e}^{-\lambda_{4i-2}(z+L)}}{1-\mathrm{e}^{-2\lambda_{4i-2}L}}\right]=0 \quad (57)$$

Also,

$$\lim_{i\to\infty}\frac{B_{i+1}}{B_i}=\lim_{i\to\infty}\left[\left(\frac{4i-2}{4i+2}\right)\frac{\left(\frac{\mathrm{e}^{\lambda_{4i+2}(z-L)}-\mathrm{e}^{-\lambda_{4i+2}(z+L)}}{\mathrm{e}^{\lambda_{4i-2}(z-L)}-\mathrm{e}^{-\lambda_{4i-2}(z+L)}}\right)}{\left(\frac{1-\mathrm{e}^{-2\lambda_{4i+2}L}}{1-\mathrm{e}^{-2\lambda_{4i-2}L}}\right)}\right]$$
$$=\mathrm{e}^{\lambda_4(z-L)}<1 \quad (58)$$

This proves that $\sum_{i=1}^{\infty}B_i$ converges absolutely. Since $\sum_{i=1}^{\infty}B_i$ converges absolutely, so does the solution in Eq. (54). Finally, the equations for velocity in Tables 1, 2 and the 3-D solution given below can all be handled as done above.

10. 3-D flow

The boundary conditions for ψ for the 3-D case are

$$\psi(x,y,0)=(1-\epsilon_1)^2$$
$$\frac{\partial\psi}{\partial x}(0,y,z)=\frac{\partial\psi}{\partial x}(a,y,z)=\frac{\partial\psi}{\partial y}(x,0,z)=\frac{\partial\psi}{\partial y}(x,b,z)=0$$
$$\psi(x,L)=(1-\epsilon_1)^2-[(1-\epsilon_1)^2-\epsilon_2^2]\times\left[U\left(x-\frac{a}{4}\right)-U\left(x-\frac{3a}{4}\right)\right]\times\left[U\left(y-\frac{b}{4}\right)-U\left(y-\frac{3b}{4}\right)\right] \quad (59)$$

The solution of Laplace's equation for ψ from separation of variables that matches the above boundary conditions is

$$\psi=(1-\epsilon_1)^2+A_0z+\sum_{i=1}^{\infty}A_i\cos(\lambda_ix)\sinh(\lambda_iz)+\sum_{j=1}^{\infty}B_j\cos(\lambda_jy)\sinh(\lambda_jz)+\sum_{i=1}^{\infty}\sum_{j=1}^{\infty}C_{ij}\cos(\lambda_ix)\times\cos(\lambda_jy)\sinh(\beta'z) \quad (60)$$

where

Table 2
3-D solution

Variable	Equation
$k_{wr}(x,y,0)$	ϵ_1
$h_o(x,y,0)$	L
$h_w(x,y,0)$	$\frac{1}{\alpha}\ln[k_{wr}(x,y,0)]+h_o(x,y,0)$
$k_{wr}(x,y,L)$	$\epsilon_1+(1-\epsilon_1-\epsilon_2)\left[U\left(x-\frac{a}{4}\right)-U\left(x-\frac{3a}{4}\right)\right]\left[U\left(y-\frac{b}{4}\right)-U\left(y-\frac{3b}{4}\right)\right]$
$h_o(x,y,L)$	$\frac{\epsilon_1-k_{wr}(x,y,L)}{\alpha}$
$h_w(x,y,L)$	$\frac{1}{\alpha}\ln[k_{wr}(x,y,L)]+h_o(x,y,L)$
λ_{4i-2}	$\frac{(4i-2)\pi}{a}$
λ_{4j-2}	$\frac{(4j-2)\pi}{b}$
β_{ij}	$\sqrt{\lambda_{4i-2}^2+\lambda_{4j-2}^2}$
ψ	$(1-\epsilon_1)^2+[(1-\epsilon_1)^2-\epsilon_2^2]\left[-\frac{z}{4L}+\frac{2}{\pi}\sum_{i=1}^{\infty}\frac{(-1)^{i+1}}{4i-2}\cos(\lambda_{4i-2}x)\frac{\sinh(\lambda_{4i-2}z)}{\sinh(\lambda_{4i-2}L)}+\frac{2}{\pi}\sum_{j=1}^{\infty}\frac{(-1)^{j+1}}{4j-2}\cos(\lambda_{4j-2}y)\frac{\sinh(\lambda_{4j-2}z)}{\sinh(\lambda_{4j-2}L)}+\frac{16}{\pi^2}\sum_{i=1}^{\infty}\sum_{j=1}^{\infty}\frac{(-1)^{i+j+1}}{(4i-2)(4j-2)}\cos(\lambda_{4i-2}x)\cos(\lambda_{4j-2}y)\frac{\sinh(\beta_{ij}z)}{\sinh(\beta_{ij}L)}\right]$
S	$1-\sqrt{\psi}$
h_o	$\frac{1}{\alpha}(\epsilon_1-S)+L-z$
h_w	$\frac{1}{\alpha}\ln S+h_o$
θ_w	$\theta_r+(\theta_s-\theta_r)S$
θ_o	$\theta_s-\theta_w$
v_{ox}	$\frac{K_{os}[(1-\epsilon_1)^2-\epsilon_2^2]}{\alpha a}\left[\sum_{i=1}^{\infty}(-1)^{i+1}\sin(\lambda_{4i-2}x)\frac{\sinh(\lambda_{4i-2}z)}{\sinh(\lambda_{4i-2}L)}+\frac{8}{\pi}\sum_{i=1}^{\infty}\sum_{j=1}^{\infty}\frac{(-1)^{i+j+1}}{4j-2}\sin(\lambda_{4i-2}x)\cos(\lambda_{4j-2}y)\frac{\sinh(\beta_{ij}z)}{\sinh(\beta_{ij}L)}\right]$
v_{wx}	$\frac{K_{ws}[(1-\epsilon_1)^2-\epsilon_2^2]}{\alpha a}\left[\sum_{i=1}^{\infty}(-1)^{i}\sin(\lambda_{4i-2}x)\frac{\sinh(\lambda_{4i-2}z)}{\sinh(\lambda_{4i-2}L)}+\frac{8}{\pi}\sum_{i=1}^{\infty}\sum_{j=1}^{\infty}\frac{(-1)^{i+j}}{4j-2}\sin(\lambda_{4i-2}x)\cos(\lambda_{4j-2}y)\frac{\sinh(\beta_{ij}z)}{\sinh(\beta_{ij}L)}\right]$
v_{oy}	$\frac{K_{os}[(1-\epsilon_1)^2-\epsilon_2^2]}{\alpha b}\left[\sum_{j=1}^{\infty}(-1)^{j+1}\sin(\lambda_{4j-2}y)\frac{\sinh(\lambda_{4j-2}z)}{\sinh(\lambda_{4j-2}L)}+\frac{8}{\pi}\sum_{i=1}^{\infty}\sum_{j=1}^{\infty}\frac{(-1)^{i+j+1}}{4i-2}\cos(\lambda_{4i-2}x)\sin(\lambda_{4j-2}y)\frac{\sinh(\beta_{ij}z)}{\sinh(\beta_{ij}L)}\right]$
v_{wy}	$\frac{K_{ws}[(1-\epsilon_1)^2-\epsilon_2^2]}{\alpha b}\left[\sum_{j=1}^{\infty}(-1)^{j}\sin(\lambda_{4j-2}y)\frac{\sinh(\lambda_{4j-2}z)}{\sinh(\lambda_{4j-2}L)}+\frac{8}{\pi}\sum_{i=1}^{\infty}\sum_{j=1}^{\infty}\frac{(-1)^{i+j}}{4i-2}\cos(\lambda_{4i-2}x)\sin(\lambda_{4j-2}y)\frac{\sinh(\beta_{ij}z)}{\sinh(\beta_{ij}L)}\right]$
v_{oz}	$\frac{K_{os}[(1-\epsilon_1)^2-\epsilon_2^2]}{\alpha}\left[\frac{1}{8L}+\frac{1}{a}\sum_{i=1}^{\infty}(-1)^{i}\cos(\lambda_{4i-2}x)\frac{\cosh(\lambda_{4i-2}z)}{\sinh(\lambda_{4i-2}L)}+\frac{1}{b}\sum_{j=1}^{\infty}(-1)^{j}\cos(\lambda_{4j-2}y)\frac{\cosh(\lambda_{4j-2}z)}{\sinh(\lambda_{4j-2}L)}+\frac{8}{\pi^2}\sum_{i=1}^{\infty}\sum_{j=1}^{\infty}\frac{(-1)^{i+j}\beta_{ij}}{(4i-2)(4j-2)}\cos(\lambda_{4i-2}x)\cos(\lambda_{4j-2}y)\frac{\cosh(\beta_{ij}z)}{\sinh(\beta_{ij}L)}\right]$
v_{wz}	$\frac{K_{ws}[(1-\epsilon_1)^2-\epsilon_2^2]}{\alpha}\left[-\frac{1}{8L}+\frac{1}{a}\sum_{i=1}^{\infty}(-1)^{i+1}\cos(\lambda_{4i-2}x)\frac{\cosh(\lambda_{4i-2}z)}{\sinh(\lambda_{4i-2}L)}+\frac{1}{b}\sum_{j=1}^{\infty}(-1)^{j+1}\cos(\lambda_{4j-2}y)\frac{\cosh(\lambda_{4j-2}z)}{\sinh(\lambda_{4j-2}L)}+\frac{8}{\pi^2}\sum_{i=1}^{\infty}\sum_{j=1}^{\infty}\frac{(-1)^{i+j+1}\beta_{ij}}{(4i-2)(4j-2)}\cos(\lambda_{4i-2}x)\cos(\lambda_{4j-2}y)\frac{\cosh(\beta_{ij}z)}{\sinh(\beta_{ij}L)}\right]$

$$\lambda_j=\frac{j\pi}{b},\quad \beta'=\sqrt{\lambda_i^2+\lambda_j^2} \tag{61}$$

The coefficients of the above equation are evaluated as before using a double half-range Fourier cosine series. Thus,

$$A_0=-\frac{(1-\epsilon_1)^2-\epsilon_2^2}{4L} \tag{62}$$

and

$$\begin{aligned}A_i&=-\frac{2[(1-\epsilon_1)^2-\epsilon_2^2]}{ab\sinh(\lambda_iL)}\int_{\frac{a}{4}}^{\frac{3a}{4}}\int_{\frac{b}{4}}^{\frac{3b}{4}}\cos(\lambda_ix)\mathrm{d}x\,\mathrm{d}y \\ &=-\frac{[(1-\epsilon_1)^2-\epsilon_2^2]}{i\pi\sinh(\lambda_iL)}\left[\sin\left(\frac{3i\pi}{4}\right)-\sin\left(\frac{i\pi}{4}\right)\right]\end{aligned} \tag{63}$$

$$\begin{aligned}B_j&=-\frac{2[(1-\epsilon_1)^2-\epsilon_2^2]}{ab\sinh(\lambda_jL)}\int_{\frac{a}{4}}^{\frac{3a}{4}}\int_{\frac{b}{4}}^{\frac{3b}{4}}\cos(\lambda_jy)\mathrm{d}x\,\mathrm{d}y \\ &=-\frac{[(1-\epsilon_1)^2-\epsilon_2^2]}{j\pi\sinh(\lambda_jL)}\left[\sin\left(\frac{3j\pi}{4}\right)-\sin\left(\frac{j\pi}{4}\right)\right]\end{aligned} \tag{64}$$

$$\begin{aligned}C_{ij}&=-\frac{4[(1-\epsilon_1)^2-\epsilon_2^2]}{ab\sinh(\beta'L)}\int_{\frac{a}{4}}^{\frac{3a}{4}}\int_{\frac{b}{4}}^{\frac{3b}{4}}\cos(\lambda_ix)\cos(\lambda_jy)\mathrm{d}x\,\mathrm{d}y \\ &=-\frac{4[(1-\epsilon_1)^2-\epsilon_2^2]}{ij\pi^2\sinh(\beta'L)}\left[\sin\left(\frac{3i\pi}{4}\right)-\sin\left(\frac{i\pi}{4}\right)\right] \\ &\quad\times\left[\sin\left(\frac{3j\pi}{4}\right)-\sin\left(\frac{j\pi}{4}\right)\right]\end{aligned} \tag{65}$$

As before, only the second and sixth term out of every eight terms in both the i and j series are nonzero, so the final result for ψ becomes

$$\begin{aligned}\psi&=(1-\epsilon_1)^2+[(1-\epsilon_1)^2-\epsilon_2^2] \\ &\quad\times\left[-\frac{z}{4L}+\frac{2}{\pi}\sum_{i=1}^{\infty}\frac{(-1)^{i+1}}{4i-2}\cos(\lambda_{4i-2}x)\frac{\sinh(\lambda_{4i-2}z)}{\sinh(\lambda_{4i-2}L)}\right. \\ &\quad+\frac{2}{\pi}\sum_{j=1}^{\infty}\frac{(-1)^{j+1}}{4j-2}\cos(\lambda_{4j-2}y)\frac{\sinh(\lambda_{4j-2}z)}{\sinh(\lambda_{4j-2}L)} \\ &\quad\left.+\frac{16}{\pi^2}\sum_{i=1}^{\infty}\sum_{j=1}^{\infty}\frac{(-1)^{i+j+1}}{(4i-2)(4j-2)}\cos(\lambda_{4i-2}x)\cos(\lambda_{4j-2}y)\frac{\sinh(\beta_{ij}z)}{\sinh(\beta_{ij}L)}\right]\end{aligned} \tag{66}$$

where

$$\beta_{ij}=\sqrt{\lambda_{4i-2}^2+\lambda_{4j-2}^2} \tag{67}$$

The solution can now be completely defined, and Table 2 contains a summary of the resulting equations.

11. Numerical results and conclusion

Equations for 1-D, 2-D, and 3-D steady-state two-phase flow have been successfully derived for an example problem. These solutions can now be used to test numerical

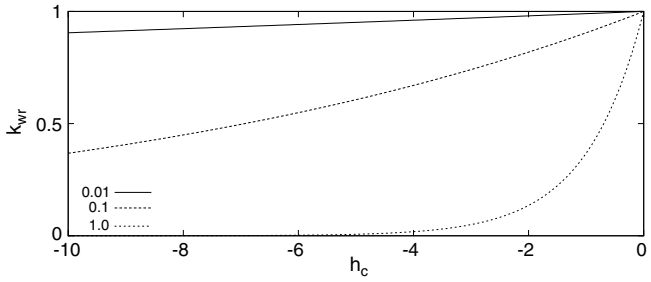

Fig. 3. Relative hydraulic conductivity for water at different values of α (m^{-1}).

models in various ways. Also, because the result only needs a solution to Laplace's equation for ψ, many other problems can be derived from this foundation.

To illustrate this potential, a simple five-point finite volume program was written for the 2-D solution given in Table 1. A Picard nonlinear solver and a conjugate gradient linear solver with diagonal preconditioning were used in this study, as these options make a good baseline reference for testing more sophisticated options such as a Newton nonlinear solver and a linear Krylov subspace solver for nonsymmetric matrices using a multigrid preconditioner. The nonlinear solver convergence criterion was when the worst grid point changed less than 10^{-3}, and the linear solver convergence criterion was when the worst grid point changed less than 10^{-6}. As shown in Fig. 3, values of $\alpha = 0.01\ m^{-1}$, $0.1\ m^{-1}$, and $1.0\ m^{-1}$ are considered for relative hydraulic conductivity. Also, $a = 10$ m, and $L = 10$ m. The larger values of α represent materials that are highly nonlinear and where the relative hydraulic conductivity of water drops quickly to near zero.

From using equally spaced grids, Tables 3–5 give accuracy and convergence results for water and oil pressure head at $x = 5$ m and $z = 0.5$ m, 5 m, and 9.5 m. As α is increased, the errors and the number of nonlinear iterations actually decrease. This is because α is in the denominator of the nonlinear terms in Eqs. (23) and (24), so the bigger α is, the less impact the nonlinear terms have on the solution. To illustrate more dramatically the effect of varying α, Tables 6–8 give results for the 161×161 grid at $x = 2.5$ m and $x = 5$ m for $\alpha = 0.01\ m^{-1}$, $0.1\ m^{-1}$, and $1.0\ m^{-1}$ near the top of the grid (rows 145–160). These results show how significantly the errors grow with smaller α near the disconti-

Table 3
Accuracy and convergence results for pressure head of water and oil at $x = 5$ m for $\alpha = 0.01\ m^{-1}$

N_x	N_y	$h_{w\text{-comp}}$	$h_{w\text{-anal}}$	Δh	$h_{o\text{-comp}}$	$h_{o\text{-anal}}$	Δh	Iterations
$z = 0.5$ m								
21	21	−147.081	−147.487	0.406	8.367	8.479	−0.112	48
41	41	−147.285	–	0.202	8.424	–	−0.056	49
81	81	−147.386	–	0.101	8.452	–	−0.028	49
161	161	−147.436	–	0.050	8.466	–	−0.014	49
$z = 5.0$ m								
21	21	−118.748	−121.384	2.636	−8.108	−6.7936	−1.315	48
41	41	−120.066	–	1.318	−7.439	–	−0.646	49
81	81	−120.726	–	0.658	−7.112	–	−0.319	49
161	161	−121.056	–	0.329	−6.952	–	−0.158	49
$z = 9.5$ m								
21	21	−84.402	−85.006	0.604	−51.525	−49.879	−1.646	48
41	41	−84.698	–	0.308	−50.684	–	−0.805	49
81	81	−84.853	–	0.154	−50.269	–	−0.390	49
161	161	−84.930	–	0.076	−50.069	–	−0.190	49

Table 4
Accuracy and convergence results for pressure head of water and oil at $x = 5$ m for $\alpha = 0.1\ m^{-1}$

N_x	N_y	$h_{w\text{-comp}}$	$h_{w\text{-anal}}$	Δh	$h_{o\text{-comp}}$	$h_{o\text{-anal}}$	Δh	Iterations
$z = 0.5$ m								
21	21	−6.158	−6.199	0.041	9.387	9.398	−0.011	42
41	41	−6.178	–	0.020	9.392	–	−0.006	42
81	81	−6.189	–	0.010	9.395	–	−0.003	43
161	161	−6.194	–	0.005	9.397	–	−0.001	43
$z = 5.0$ m								
21	21	−7.375	−7.638	0.264	3.689	3.821	−0.131	42
41	41	−7.506	–	0.132	3.756	–	−0.065	42
81	81	−7.572	–	0.066	3.789	–	−0.032	43
161	161	−7.605	–	0.033	3.805	–	−0.016	43
$z = 9.5$ m								
21	21	−7.990	−8.051	0.060	−4.703	−4.538	−0.165	42
41	41	−8.020	–	0.031	−4.618	–	−0.081	42
81	81	−8.035	–	0.015	−4.577	–	−0.039	43
161	161	−8.043	–	0.008	−4.557	–	−0.019	43

Table 5
Accuracy and Convergence Results for Pressure Head of Water and Oil at $x = 5$ m for $\alpha = 1.0\ \mathrm{m}^{-1}$

N_x	N_y	$h_{\text{w-comp}}$	$h_{\text{w-anal}}$	Δh	$h_{\text{o-comp}}$	$h_{\text{o-anal}}$	Δh	Iterations
$z = 0.5$ m								
21	21	7.9343	7.9301	0.0042	9.4887	9.4898	−0.0011	34
41	41	7.9322	–	0.0021	9.4892	–	−0.0006	35
81	81	7.9312	–	0.0010	9.4895	–	−0.0003	35
161	161	7.9307	–	0.0007	9.4897	–	−0.0001	35
$z = 5.0$ m								
21	21	3.7629	3.7362	0.0268	4.8689	4.8821	−0.0131	34
41	41	3.7497	–	0.0135	4.8756	–	−0.0064	35
81	81	3.7431	–	0.0070	4.8789	–	−0.0032	35
161	161	3.7400	–	0.0038	4.8805	–	−0.0015	35
$z = 9.5$ m								
21	21	−0.3490	−0.3551	0.0061	−0.0203	−0.0038	−0.0165	34
41	41	−0.3520	–	0.0031	−0.0119	–	−0.0081	35
81	81	−0.3535	–	0.0016	−0.0077	–	−0.0039	35
161	161	−0.3543	–	0.0008	−0.0057	–	−0.0019	35

Table 6
Difference in finite volume and analytical solution for pressure head of water and oil at $x = 2.5$ m and $x = 5$ m for $\alpha = 0.01\ \mathrm{m}^{-1}$ for the 161 × 161 grid

Row	Δh_{w} (2.5)	Δh_{w} (5)	Δh_{o} (2.5)	Δh_{o} (5)
145	0.8744	0.1598	−0.6128	−0.2500
146	0.9218	0.1496	−0.6508	−0.2451
147	0.9764	0.1393	−0.6946	−0.2396
148	1.0398	0.1289	−0.7455	−0.2335
149	1.1143	0.1184	−0.8053	−0.2266
150	1.2030	0.1079	−0.8765	−0.2189
151	1.3101	0.0973	−0.9626	−0.2103
152	1.4418	0.0868	−1.0687	−0.2008
153	1.6074	0.0763	−1.2026	−0.1903
154	1.8219	0.0660	−1.3768	−0.1785
155	2.1105	0.0558	−1.6128	−0.1654
156	2.5205	0.0458	−1.9513	−0.1506
157	3.1515	0.0360	−2.4801	−0.1336
158	4.2493	0.0266	−3.4250	−0.1137
159	6.5273	0.0174	−5.5025	−0.0892
160	12.2659	0.0086	-11.6640	−0.0563

Table 7
Difference in finite volume and analytical solution for pressure head of water and oil at $x = 2.5$ m and $x = 5$ m for $\alpha = 0.1\ \mathrm{m}^{-1}$ for the 161 × 161 grid

Row	Δh_{w} (2.5)	Δh_{w} (5)	Δh_{o} (2.5)	Δh_{o} (5)
145	0.0880	0.0160	−0.0611	−0.0250
146	0.0928	0.0150	−0.0649	−0.0245
147	0.0982	0.0140	−0.0693	−0.0240
148	0.1046	0.0129	−0.0744	−0.0234
149	0.1120	0.0119	−0.0804	−0.0227
150	0.1209	0.0108	−0.0875	−0.0219
151	0.1316	0.0098	−0.0961	−0.0210
152	0.1448	0.0087	−0.1067	−0.0201
153	0.1613	0.0077	−0.1201	−0.0190
154	0.1828	0.0066	−0.1375	−0.0179
155	0.2116	0.0056	−0.1611	−0.0166
156	0.2526	0.0046	−0.1949	−0.0151
157	0.3157	0.0036	−0.2478	−0.0134
158	0.4254	0.0027	−0.3423	−0.0114
159	0.6531	0.0017	−0.5501	−0.0089
160	1.2268	0.0009	−1.1662	−0.0057

Table 8
Difference in finite volume and analytical solution for pressure head of water and oil at $x = 2.5$ m and $x = 5$ m for $\alpha = 1.0\ \mathrm{m}^{-1}$ for the 161 × 161 grid

Row	Δh_{w} (2.5)	Δh_{w} (5)	Δh_{o} (2.5)	Δh_{o} (5)
145	0.0096	0.0017	−0.0060	−0.0025
146	0.0101	0.0016	−0.0064	−0.0025
147	0.0106	0.0015	−0.0068	−0.0024
148	0.0112	0.0013	−0.0073	−0.0023
149	0.0120	0.0012	−0.0079	−0.0023
150	0.0129	0.0011	−0.0086	−0.0022
151	0.0139	0.0010	−0.0095	−0.0021
152	0.0153	0.0009	−0.0105	−0.0020
153	0.0169	0.0008	−0.0118	−0.0019
154	0.0190	0.0007	−0.0136	−0.0018
155	0.0219	0.0006	−0.0159	−0.0017
156	0.0260	0.0005	−0.0193	−0.0015
157	0.0323	0.0004	−0.0246	−0.0014
158	0.0432	0.0003	−0.0340	−0.0012
159	0.0659	0.0002	−0.0548	−0.0009
160	0.1230	0.0001	−0.1165	−0.0006

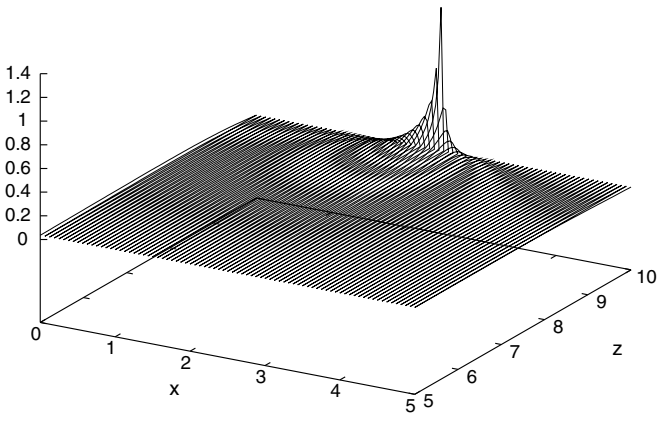

Fig. 4. Surface plot of difference in finite volume solution and analytical solution for pressure head of water for the upper, left-hand corner of the grid for $\alpha = 0.1\ \mathrm{m}^{-1}$ using the 161 × 161 grid.

nuities as compared to the middle of the grid. Fig. 4 gives a surface plot of error in the pressure head of water (finite

volume solution – analytical solution) for the upper, left-hand part of the grid to further illustrate the concentration of error near the $x = 2.5$ m, $z = 10$ m discontinuity. These results also show that for a given value of α, the number of nonlinear iterations remains almost constant while increasing the grid size.

Other tests such as grid adaptivity near the top of the soil sample can also be done. The above results show that the presented solutions can certainly aid the verification process of a two-phase flow groundwater program.

Acknowledgement

This work was supported in part by a grant of computer time from the Department of Defense High Performance Computing Modernization Program at the US Army Engineer Research and Development Center (ERDC) Major Shared Resource Center, Information Technology Laboratory, Vicksburg, Mississippi, USA, and an In-house Laboratory Independent Research project from ERDC.

References

Cai, R., Zhang, D., 2001. Some explicit analytical solutions of unsteady two phase flow. Chinese J. Mech. Eng. 37, 1–38.

Gardner, W.R., 1958. Some steady-state solutions of the unsaturated moisture flow equation with application to evaporation from a water table. Soil Sci. 85, 228–232.

Hewett, T.A., Yamada, T., 1997. Theory for the semi-analytical calculation of oil recovery and effective relative permeabilities using streamtubes. Adv. Water Resour. 20, 279–292.

Hou, T.Y., 2005. Multiscale modelling and computation of fluid flow. Int. J. Numer. Methods Fluids 47, 707–719.

Iqbal, G.M., Civan, F., 1986. Reservoir simulation based on the finite analytic method. In: Society of Petroleum Engineers of AIME, 61st Annual Technical Conference and Exhibition of the Society of Petroleum Engineers, New Orleans, LA, USA.

Irmay, S., 1954. On the hydraulic conductivity of unsaturated soils. Eos Trans. AGU 35.

Jinno, K., 1978. Equations of free surface and two-phase interface in ground water flow. Memoirs Faculty Eng., Kyushu Univ. 38, 177–199.

Okusu, N.M., Udell, K.S., 1989. Immiscible displacement in porous media including gravity and capillary forces. Am. Soc. Mech. Eng. Fluids Eng. Div. 82, 13–21.

Panfilov, M., Floriat, S., 2004. Nonlinear two-phase mixing in heterogeneous porous media. Transp. Porous Media 57, 347–375.

Sander, G.C., Parlange, J.Y., Kuhnel, V., Hogarth, W.L., Lockington, D., O'Kane, J.P.J., 1988. Exact nonlinear solution for constant flux infiltration. J. Hydrol. 97, 341–346.

Seǵol, G., 1994. Classic Groundwater Simulations. Prentice Hall, Englewood Cliffs, NJ, p. 352.

Tracy, F.T., 1997. Evaluation of the non-isothermal/thermal unsaturated/saturated flow and transport (NUFT) code using analytical solutions. In: Proceedings, Congress of the International Association of Hydraulic Research, Groundwater: An Endangered Resource, 1997, pp. 427–432.

Tracy, F.T., 2006. Clean two- and three-dimensional analytical solutions of Richards' equation for testing numerical solvers. Water Resour. Res. 42, W08503.

Tsai, S., 1990. Analytic solution of dense two-phase flow in a vertical pipeline. Appl. Math. Mech. 11, 1095–1103.

van Genuchten, M., 1980. A closed-form equation for producing the hydraulic conductivity of unsaturated soils. Soil Sci. Am. J. 44, 892–898.

Verma, A.P., Mishra, S.K., 1973. Similarity solution for instabilities in double-phase flow through porous media. J. Appl. Phys. 44, 1622–1624.

Walter, S.A., 1990. Coupling coefficients for two-phase flow in pore spaces of simple geometry. Transp. Porous Media 5, 97–102.

Warrick, A.W., 2003. Soil Water Dynamics. Oxford Univ. Press, New York, pp. 247–258.

Yang, W., 1992. Analytical solution to two-phase flow in porous media and its application to water coning. Society of Petroleum Engineers of AIME, pp. 1–35.